

# AGN outflows in a Cosmological Context

Robyn Levine and Nickolay Y. Gnedin

*Center for Astrophysics & Space Astronomy, University of Colorado, Boulder, CO 80309*

robyn.levine@colorado.edu, gnedin@casa.colorado.edu

## ABSTRACT

We combine cosmological simulations with an AGN luminosity function constrained by optical surveys in order to create a realistic AGN distribution in which to model AGN outflows. The outflows are modeled with assumptions of spherical symmetry and energy conservation. We study the importance of the kinetic luminosity of AGN outflows in determining the fractional volume of the IGM filled with outflows as a function of redshift. We find that kinetic luminosities of  $< 10\%$  of the bolometric luminosities are required or the entire IGM would be filled with outflows at  $z = 0$ . We also examine the effects of varying the AGN lifetime and the bias parameter, which describes how tightly correlated AGN are to high density regions. We find that longer lifetimes ( $\tau_{AGN} \sim 1$  Gyr), as well as small bias parameters increase the filling fraction.

*Subject headings:* cosmology: theory—galaxies: active—intergalactic medium—large-scale structure of universe—quasars: general

## 1. INTRODUCTION

Outflows from active galactic nuclei (AGN) potentially play a very significant role in the evolution of large-scale structure. Such outflows consist of hot, tenuous out-flowing gas detected in absorption, and the powerful radio jets detected in some quasars. Blue-shifted absorption lines (relative to systematic velocity of the AGN), such as  $\text{Ly}\alpha$  and the C IV and N V doublets, indicate gas moving away from the central source at high velocities (Ulrich 1988; Crenshaw et al. 1999). Broad absorption lines (BAL) indicating even higher velocities, are detected in luminous AGN (e.g., Hewett & Foltz 2003). Radio-loud quasars (RLQ) also carry substantial amounts of energy into the intergalactic medium (IGM) via collimated jets of relativistic plasma (e.g., Begelman, Blandford, & Rees 1984). AGN outflows may play a role in distributing magnetic fields into the IGM (e.g., Furlanetto & Loeb 2001), and they can impact the evolution of their host galaxies by, for example, regulating the

growth of supermassive black holes (Wyithe & Loeb 2003). BAL outflows and RLQ are also possible mechanisms for heating the intra-cluster medium (e.g., Valageas & Silk 1999; Nath & Roychowdhury 2002). The magnitude of the influence of outflows on the IGM depends on a few key properties of AGN, such as the relationship between kinetic and bolometric luminosity, that still need to be constrained by observation.

In RLQ, the kinetic luminosity of the jet is thought to be correlated with the bolometric luminosity (Willott et al. 1999). Direct estimates of the kinetic luminosity in BAL outflows can be made if such quantities as the covering fraction of the outflows, the outflow velocity, the radius of the outflow, and the column density are known. The velocities are accurately obtained from the absorption lines, and the covering fractions can be estimated with statistical arguments (Weymann 1997). The radius of the outflow can be obtained through observations of the photoionizing flux of the central source (Krolik 1999). Estimates of the column densities can be made by studying the UV and X-ray absorption lines (Gallagher et al. 1999, 2001). Uncertainties in the above quantities translate to uncertainties in the kinetic luminosity, and therefore into uncertainties in the energy of AGN outflows. More energetic outflows can fill a larger volume, having a greater impact on large-scale structure.

In this paper, we model the growth of AGN outflows using energy conservation arguments and simple approximations about their geometry. Through numerical simulations we model the distribution of these outflows and hence we can estimate the degree to which they affect the universe on global scales, or the fractional volume occupied by AGN outflows. In §2, we describe some of the details of the cosmological simulation and the luminosity function that we have combined to obtain an AGN distribution. In §3 we explain the assumptions surrounding our physical model of the growth of heated bubbles around AGN as well as our selection of kinetic luminosity. In §4, we show the advantage of using a simulated density distribution over using simple statistical methods for the distribution of AGN. In §5 we examine the effects of simulation size and resolution, AGN lifetime, and AGN bias on the cumulative effect of outflows, and we conclude in §6. For the rest of this paper, we assume  $\Omega_m = .27$ ,  $\Omega_\Lambda = 0.73$ , and  $\Omega_b = .04$  with  $\Omega_b h^2 = 0.02$ , consistent with the WMAP data.

## 2. SIMULATING THE AGN ENVIRONMENT AND DISTRIBUTION

In order to understand the influence of AGN outflows on a global scale, it is useful to model the outflows in the context of large-scale structures. We assume here that AGN trace high density regions, and so use a gas density distribution to bias AGN in our study. Other studies have, for example, approximated the distribution of AGN with statistical formulae. Tegmark, Silk, & Evrard (1993) and Furlanetto & Loeb (2001; hereafter, F & L) both use

Poisson distributions to model the spatial distribution of galaxies for simplicity, in order to obtain filling fractions of supernova-driven winds and of AGN outflows respectively. We combine a  $z$ -dependent luminosity function with a simulated gas density distribution, allowing us to consider the AGN in their appropriate environments rather than homogeneously distributing them throughout the universe. In §4, we compare a Poisson distribution of AGN outflows with our model.

## 2.1. Cosmological Density Distribution

In order to model the evolution of the gas density distribution in the universe, we use a standard Particle-Mesh code to simulate the distribution of the dark matter, and we assume that on the scales we are considering, the gas distribution follows that of the dark matter, which is supported by cosmological gas dynamics simulations (Gnedin 2000; Chiu & Ostriker 2000; Miller & Ostriker 2001; Somerville 2002; Tassis et al. 2003; Benson & Madau 2003; Susa & Umemura 2004; Shapiro, Iliev, & Raga 2004; Mo & Mao 2004). We also assume that the temperature of the cosmic gas is constant at 15,000 K. This assumption is, clearly, an oversimplification, since the temperature of the cosmic gas is known to evolve with time (Ricotti, Gnedin, & Shull 2000; Schaye et al. 2000; McDonald et al. 2001; Kim, Cristiani, & D’Odorico 2002; Theuns et al. 2002; Hui & Haiman 2003) and vary in space. However, since the typical sizes of AGN-driven bubbles are significantly larger than the scales over which the temperature of cosmic gas changes, this approximation is sufficient for our purposes.

## 2.2. Luminosity Function

The above simulation produces a gas density distribution at each time step, from  $z \sim 19$  to  $z = 0$ . In each step, we use a luminosity function to populate the simulation with AGN over a range of luminosities. In order to place AGN into our simulation, we must implement an AGN luminosity function that applies to high redshifts. The scarcity of high- $z$  galaxy detections in surveys makes luminosity function predictions difficult, although the ability to make detections is improving. We use a model by Schirber & Bullock (2003) for the QSO luminosity function. The model satisfies all existing constraints from optical surveys, such as the Sloan Digital Sky Survey (SDSS) data and the Great Observatories Origins Deep Survey (GOODS) data for  $z > 3$  (Fan et al. 2001a, 2001b; Cristiani et al. 2004) and Two Degree Field (2dF) data for  $z < 2.3$  (Boyle et al. 2000). It should be noted that optical surveys perhaps underestimate the faint-end, low- $z$  luminosity function. Hard X-ray detections of AGN yield a higher number of faint AGN at low-redshift than in previous optical surveys

(Barger et al. 2005). The model that we use for now parameterizes the following luminosity function:

$$\phi(L_B, z) = \frac{\phi_*/L_*}{(L_B/L_*)^{\gamma_f} + (L_B/L_*)^{\gamma_b}} . \quad (1)$$

In the above equation,  $\phi_*$  is the average comoving number density of AGN,  $L_*$  and  $L_B$  are the break luminosity and AGN B-band luminosities respectively (given in units of  $L_{\odot,B}$  where we have followed S & B in using  $2.11 \times 10^{33} \text{ ergs s}^{-1}$  for the B-band luminosity of the sun), and  $\gamma_f$  and  $\gamma_b$  are the faint and bright-end slopes respectively. As in S & B, we interpolate the SDSS and 2dF fits for  $2.3 < z < 3$ . The parameterization is given in Table 1, and the luminosity function for several different redshifts is plotted in Figure 1. Note that for  $z > 3$ ,  $L_*$  and  $\phi_*$  depend on the weighted emissivity of AGN (accounting for contributions to the ionizing rate from other sources, such as stars). The weighted emissivity is given by  $\log_{10} \hat{\epsilon}^Q = -0.245z + 0.596$ , a simple power law fit to the values given in S & B Table 1. We have chosen a minimum AGN luminosity of  $10^8 L_{\odot,B}$  as in S & B, who argue that this represents the faintest Seyfert galaxies found. We extrapolate the high- $z$  parameterization of Table 1 to  $z \sim 19$ , which introduces a significant uncertainty in the abundance of AGN at high redshift. However, as we show below, AGN at  $z < 3$  dominate, so this uncertainty affects our results insignificantly. The exact redshift range for each run depends on the size of the simulation box since larger boxes can sample an earlier, rarer population of AGN.

It should be noted that we used S & B’s “Model A” to determine this particular luminosity function for  $z \geq 3$ . The model uses the emissivity of the ionizing background, assuming a stellar as well as an AGN contribution, to constrain the AGN luminosity function in combination with the SDSS data. The model implements the ionizing rates of McDonald & Miralda-Escudé (2001) and assumes an escape fraction of 0.16 (including the stellar contribution to the ionizing background). The model neglects optically obscured AGN on the basis

Table 1. Parameterization of luminosity function

	$z < 2.3$	$2.3 < z < 3$	$z > 3$
$\log_{10} (\phi_{\star} \text{ Gpc}^3)$	3.029	$-0.87z + 5.02$	$2.80 + 2.72 \log_{10} \hat{\epsilon}^Q(z) + 0.81 (z - 3)$
$\log_{10} (L_{\star} L_{\odot,B}^{-1})$	$11.24 + 1.36z - 0.27z^2$	$-0.72z + 14.6$	$12.2 - 1.72 \log_{10} \hat{\epsilon}^Q(z) - 0.81 (z - 3)$
$\gamma_b$	3.41	$-1.19 z + 6.14$	2.58
$\gamma_f$	1.58	1.58	1.58

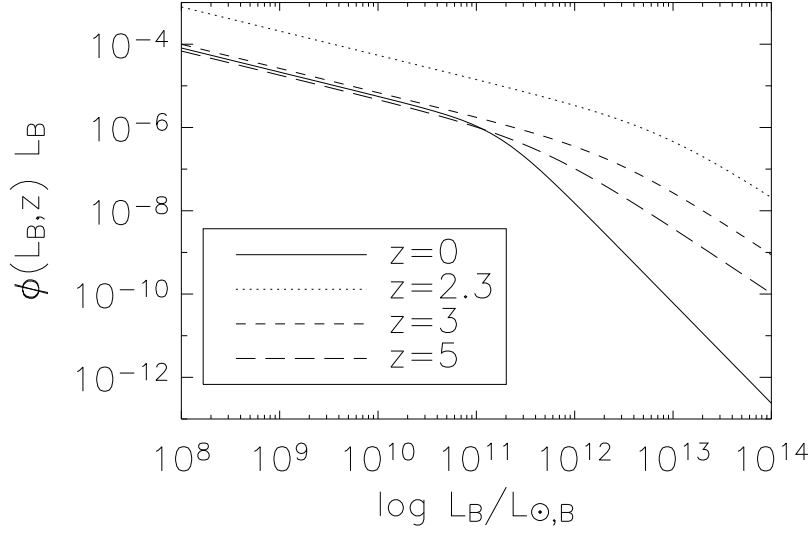


Fig. 1.— Calculated comoving number density of AGN at a given redshift, using a luminosity function consistent with 2dF, SDSS and GOODS data.

that they do not make a significant contribution to the ionizing background. This means that the luminosity function we use could be excluding some AGN that host outflows. Of the models described by S & B, we have chosen ‘Model A’ because it is most consistent (of the models studied by S & B) with the faint end luminosity function (for  $z > 4$ ), from GOODS (Cristiani et al. 2004).

We use the luminosity function to calculate the number of AGN at a given redshift and luminosity in each simulation box, and we then place each one into a random location, but with a bias toward high density regions. In order to distribute AGN so that they correspond to regions of high density, we calculate, for each cell, the probability of hosting an AGN given by

$$P(i, j, k) = \frac{\rho_m^\alpha(i, j, k) \Delta V}{\sum_{i, j, k=0}^{N-1} (\rho_m^\alpha \Delta V)} . \quad (2)$$

Above,  $\rho_m$  is the matter density (in units of average baryon density) in each cell specified by coordinates  $i, j, k$ ;  $N$  is the size of simulation box;  $\Delta V$  is the comoving volume of each cell; and  $\alpha$  is a bias parameter ensuring that regions of higher density are more likely to host AGN. The above probability function is independent of the characteristics of individual AGN (such

as luminosity). Analysis of existing observations suggests that AGN are more biased toward high density regions at increasing redshifts (e.g., Croom et al. 2004; Porciani, Magliocchetti, & Norberg 2004). In §5.3, we will examine the effects of different bias parameters on our results. In order to place the AGN in specific cells, we randomly choose a cell and compare the value of  $P(i, j, k)$  in that cell to a randomly generated number between zero and one. If  $P(i, j, k)$  is greater than the random number, an AGN goes into the cell. Otherwise, the process repeats until the AGN has been placed in the simulation. This method has the effect of biasing AGN toward regions of higher density, while fully allowing for Poisson noise in their distribution.

### 3. AGN OUTFLOWS

The following sections detail the distribution and kinematics of AGN outflows in our model. Outflows are not observed in all AGN, and so §3.1 deals with our method of selecting AGN to host outflows. In §3.2, we describe our assumptions about the expansion and evolution of individual outflows into the IGM, and in §3.3, we discuss the effects of kinetic luminosity on the outflows.

#### 3.1. Distribution of Outflows

In our model we assume that the AGN produce outflows that are responsible for distributing tenuous, hot gas into the IGM. The outflows may also be a mechanism for depositing metals and magnetic fields into the IGM. However, outflows are only associated with a fraction of AGN, which we must reflect in our model. Detection of blue-shifted broad absorption lines in an AGN’s spectrum indicates out-flowing gas from the nucleus. Until fairly recently, observations indicated that these broad absorption lines were limited to radio-quiet quasars (Stocke et al. 1992), and only seen in  $\sim 10\%$  of them. However, recent detections of BAL outflows in RLQ (e.g., Brotherton et al. 1998; Menou et al. 2001) suggest that BAL outflows do not necessarily follow this radio dichotomy. There is, however, evidence for some luminosity dependence in the occurrence of BAL outflows. Crenshaw et al. (1999) examined the UV spectra of several Type I Seyfert galaxies obtained with the Hubble Space Telescope, and found intrinsic, narrow absorption lines in more than half of their sample. The absorption spectra of these low-luminosity objects show similarities to the BAL features in high-luminosity objects, suggesting a possible relationship between the two. On the higher luminosity end, Hewett & Foltz (2003) apply a magnitude correction to the Large Bright Quasar Survey (LBQS; Hewett, Foltz, & Chaffee 1995, 2001) and find a higher percentage

of BAL quasars than previously determined. Magnitude and flux-limited samples can exclude BAL quasars in which the absorbing gas reduces the spectral energy distribution of the quasars in the wavelength range of selection. After applying a correction for this effect, Hewett & Foltz find that  $\sim 20\%$  of the AGN in the sample host outflows.

In our model, we interpolate the above low and high-luminosity limits for the fraction of AGN hosting outflows,  $f_{out}$ , and combine this fraction with the luminosity function of §2.2. Our formulation is as follows:

$$f_{out} = \begin{cases} .5 & \text{for } \log L_B < 10 , \\ 1.5 - 0.1 \log L_B & \text{for } 10 \leq \log L_B \leq 13 , \\ .2 & \text{for } \log L_B > 13 , \end{cases} \quad (3)$$

where the lower and higher-end luminosities are consistent with the fractions determined above. It is not well known whether the above statistics also apply to the population of X-ray detected AGN without optical counterparts. However, because X-ray surveys detect more low-luminosity AGN than optical surveys, it is possible that there are more AGN containing outflows than we here assume. Additionally, it should be noted that because of the range of covering fractions of AGN outflows, the fraction of AGN hosting outflows could be larger than what is observed, even in optical surveys, due to orientation effects (Morris 1988; Weymann et al. 1991; Hamann, Korista, & Morris 1993). Therefore, our assumptions should provide a conservative lower limit to the number of AGN hosting outflows.

### 3.2. Evolution of Outflows

In order to understand the degree to which active galaxies affect the IGM, it is important to have an accurate model of the expansion of hot, ionized gas into the IGM. The environment of the outflow must be considered in order to model the expansion. Using the density profile described in §2, we can, to a degree, reproduce the environment surrounding each of the individual active galaxies that we placed in our simulation in accordance with the luminosity function (eq. 1) and  $f_{out}$  (eq. 3).

The lifetime of the active galactic nucleus is short compared to the expansion time of the bubbles, which lasts over the duration of our simulation. Therefore, we consider the active phase as a brief energy injection, followed by an adiabatic blast wave gathering up material in the IGM, analogous to the adiabatic phase of a supernova remnant. As in Scannapieco & Oh (2004), we have used the familiar Sedov-Taylor blast wave model to determine the size

of the bubbles in our analysis. Their Equation 10, which we adopt for convenience of units, follows:

$$R_s = (1.7 \text{ Mpc}) \left( \frac{E_k}{10^{60} \text{ ergs}} \right)^{1/5} (1 + \delta_m)^{-1/5} (1 + z)^{-3/5} \left( \frac{t_{age}}{10^9 \text{ yr}} \right)^{2/5}. \quad (4)$$

In the above equation,  $E_k$  is the kinetic energy injected by the AGN,  $\delta_m$  is the overdensity, and  $t_{age}$  is the time since the active phase began. The overdensity is an average over all cells within the radius of the bubble, obtained using an iterative technique. The above Sedov-Taylor solution, with a constant density, is clearly not valid as the outflow escapes its host galaxy and travels first through a region with a steeply-falling off density profile, e.g. the NFW profile (Navarro, Frenk, & White 1997). However, our simulation does not resolve this stage of the expansion. The virial radius of a typical  $L_*$  galaxy is well below the resolution of our simulation. Without modeling the expansion of the outflows inside this region, there is uncertainty in the speed with which the outflows escape their host galaxies. However, this uncertainty is hidden by the parameter  $E_k$ , which describes the actual energy input from the AGN.

We assume that the bubbles expand according to the above equation until they reach a pressure equilibrium with their environment. If pressure equilibrium is reached before the energy injection has stopped, the growth of the bubbles is determined by the surrounding pressure and the injected energy, and the size is given by

$$R_P = (3.24 \times 10^{-25} \text{ Mpc}) \left( \frac{3E_k}{4\pi P} \right)^{1/3}. \quad (5)$$

The pressure of the surrounding medium is given by  $P = (1 + \delta_m)\bar{n}_b k_b T$ , where the quantity  $(1 + \delta_m)\bar{n}_b$  is the average gas density inside the bubble as determined above, and  $T = 1.5 \times 10^4 \text{ K}$  (the average temperature of the IGM). The kinetic energy in Equations 4 and 5 is given by  $E_k = \varepsilon_{kB} L_B t_{age}$  where  $t_{age}$  is the age of the AGN during the active phase, or the lifetime of the AGN once the active phase has ended. We assume a constant lifetime of  $10^8 \text{ yrs}$  for all AGN until §5.2 in which we will examine other lifetimes. The parameter  $\varepsilon_{kB}$  is given by the ratio of the kinetic luminosity of the outflow to the AGN B-band luminosity ( $L_k/L_B$ ). Each AGN injects kinetic energy into the IGM at a rate ( $L_k$ ) correlated with the AGN's luminosity. We assume that the AGN are accreting at roughly their Eddington rates, so that  $L_{edd} \sim L_{bol}$ . As in F & L, we adopt  $L_{bol} \sim 10L_B$ , consistent with Elvis et al. (1994). We describe our choice of the kinetic fraction,  $L_k/L_{bol}$  or  $\varepsilon_k$ , in the next section.

After the energy injection phase, bubbles in pressure equilibrium no longer expand as



a result of the energy injection of the AGN. Any subsequent evolution of the bubbles in our simulation is determined by the Hubble expansion and the evolution of the density distribution in the surrounding environment. Overlap of the bubbles is not likely to affect the expansion significantly. When an expanding bubble in pressure equilibrium overlaps with the interior of another bubble, encountering densities much lower than those typical in the IGM, the expansion speed does not change, as there is no longer a pressure gradient.

Our model does not include radiative cooling, as the cooling times for these bubbles are typically much longer than the timescales we consider. However, for bubbles located in cluster environments (higher densities and temperatures, etc.), radiative cooling, as well as other physical processes, may become important. Accurately modeling outflow physics in these complex environments requires the use of hydrodynamical simulations. Separate work is currently underway to understand the impact of AGN outflows in these environments (e.g., Brüggen & Kaiser 2002; Ruszkowski, Brüggen, & Begelman 2004).

Figure 2 shows the evolution of the bubble size for two typical AGN (each with luminosities of  $\sim 10^9 L_{\odot,B}$ ) residing in different environments within the simulation. The figure shows that the AGN residing in the lower density environment produces a larger bubble ( $\sim 4.8 h^{-1}$  Mpc) than the AGN in the higher density environment ( $\sim 2.2 h^{-1}$  Mpc).

In both F & L and Nath and Roychowdhury (2002), AGN outflows are treated as collimated jets that spread out into a cocoon after reaching pressure equilibrium at the end of the AGN’s active phase. Furthermore, both BAL AGN and RLQ are treated similarly, justified by the small covering fraction of BAL outflows, averaging at around 10% (Weymann 1997). We likewise adopt the practice of treating the two different objects similarly, noting that there is additional incentive in the likelihood of overlap between RLQ and BAL AGN. Furthermore, because the time scales we consider are significantly longer than the AGN injection phase, we do not model collimated jets, but rather approximate the outflows as bubbles expanding into the IGM with spherical symmetry. However, as demonstrated by Figure 2 of F & L, if the energy injection is modeled assuming spherical symmetry during the active phase, rather than with collimated jets, the result is only a slightly smaller final comoving bubble size. The entirely spherical case produces a smaller cocoon because the surface area of the bubble causes it to decelerate sooner, whereas a collimated jet makes its way through the IGM more easily.

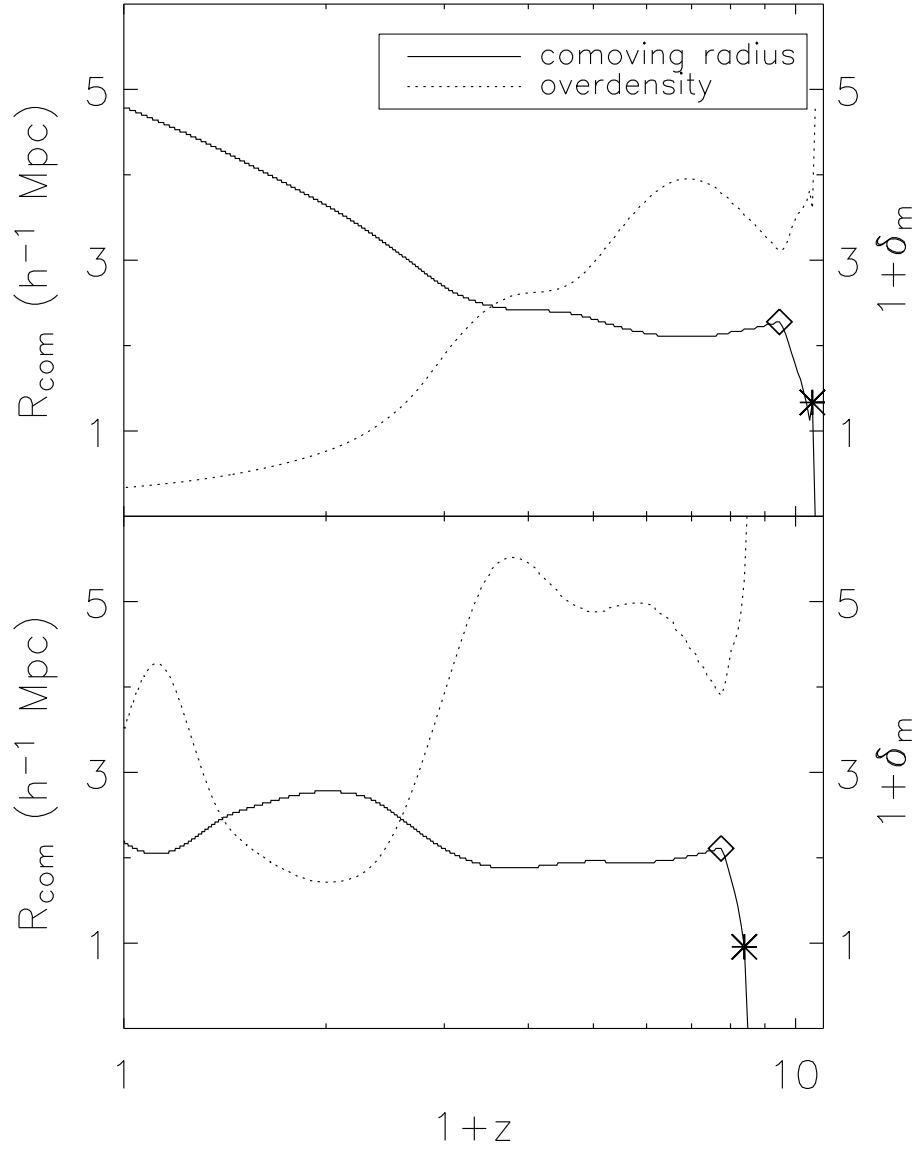


Fig. 2.— Overlay of the comoving radius of two AGN bubbles (*solid*) in different environments, and the average overdensity,  $1 + \delta_m$ , inside each bubble (*dotted*). We have chosen AGN with luminosities of  $\sim 10^9 L_{\odot,B}$ . We show the point at which the bubbles reach pressure equilibrium with their environments (*star*) and the end of the active phase after a lifetime of  $10^8$  yrs (*diamond*). The figures represent typical AGN, although the exact behavior is a function of luminosity and environment. Note that the continued growth of the bubble after reaching pressure equilibrium is a result of the continuing energy injection from the nucleus. Once the energy injection (active phase) ends, the bubble size only changes with the evolution of its environment and the Hubble flow. In the top figure, the bubble is expanding into a region of lower density, allowing the expansion to continue. In the bottom figure, the bubble expands into a denser region, eventually halting the expansion.

### 3.3. Kinetic Luminosity and Filling Fraction

Estimates of the kinetic fraction,  $\varepsilon_k$ , are subject to a number of observational uncertainties surrounding BAL outflows. Observational constraints depend on quantities that are difficult to determine, such as the distance of outflows from the central source, and the covering fraction of the outflows (e.g., De Kool et al. 2001). We use our model of AGN outflows to calculate the filling fraction of outflows as a function of redshift,  $F(z)$ , for a box of length  $128 h^{-1} \text{ Mpc}$  (with  $0.5 h^{-1} \text{ Mpc}$  cells), assuming that all of the AGN are active for  $10^8 \text{ yrs}$ , and that they follow a constant bias,  $\alpha = 2$ . We then treat the kinetic fraction as a free parameter of our model. We start with  $\varepsilon_{kB} = 1$ , or a kinetic fraction  $\varepsilon_k = 0.1$ , as in F & L. Nath & Roychowdhury (2002) argue that  $\varepsilon_k = 0.1$  is probably an upper limit for BAL outflows, assuming that the covering fraction of BAL outflows is  $\sim 10\%$ . Figure 3 shows the fractional volume filled with AGN outflows for decreasing kinetic fraction. We find that using a kinetic fraction of 10%, the entire simulation box is filled with outflows by  $z \sim 2$ . Similarly, Scannapieco & Oh (2004) find that a kinetic fraction of 10% overestimates feedback effects in their model of AGN outflows.

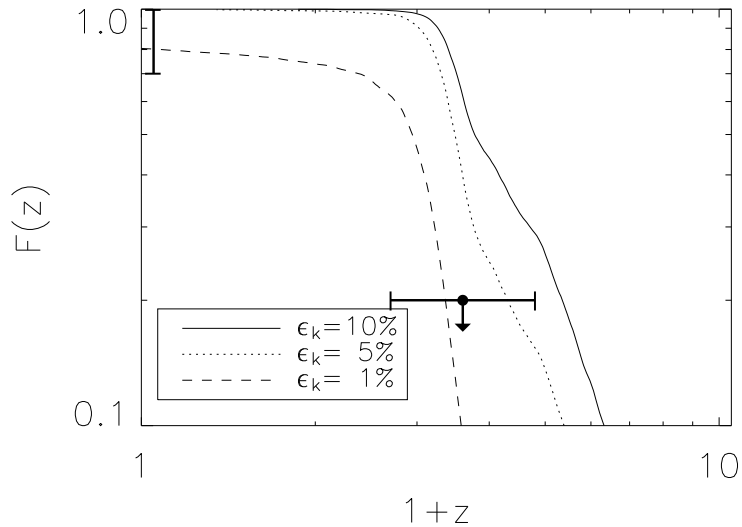


Fig. 3.— Fractional volume filled with AGN outflows as a function of redshift for different kinetic fractions. The bars represent the observational constraints on the filling fraction of AGN outflows from the Ly $\alpha$  forest, as discussed in the text.

Knowledge of the filling fraction of the Ly $\alpha$  forest at various redshifts can provide further constraints, if we assume that the AGN outflows consist of hot, tenuous gas that cannot

occupy the same volume of space as Ly $\alpha$  absorbing regions. At low- $z$ , simple conclusions drawn from observations of the Ly $\alpha$  forest constrain the fractional volume of voids to between 70 and 99.6% of the total volume, providing an upper limit to the filling fraction of AGN outflows (e.g., Penton, Stocke, & Shull 2004; Davé et al. 1999). The vertical bar near  $z = 0$  in Figure 3 shows the constrained filling fraction of voids. An  $\varepsilon_k$  of less than 10% produces filling factors that are consistent with the above values, but imposing more precise constraints from Ly $\alpha$  forest observations is difficult because of the range of column densities under consideration. For somewhat higher redshifts ( $1.7 < z < 3.8$ ), Duncan, Ostriker, & Bajtlik (1989) have studied voids in the Ly $\alpha$  forest and determined that voids with sizes between 10 and 70  $h^{-1}$  Mpc occupy  $< 20\%$  of the volume. The horizontal bar in Figure 3 shows this upper limit for the filling fraction of AGN outflows over the appropriate redshift range. We choose  $\varepsilon_{kB} = .1$  ( $\varepsilon_k = 1\%$ ) as our fiducial value, as it seems to match observational and theoretical constraints more closely than the higher values.

#### 4. COMPARISON WITH A POISSON DISTRIBUTION

As previously mentioned, it is possible to calculate the filling fraction of AGN outflows analytically by assuming that AGN are distributed according to Poisson statistics. In this section, we demonstrate the advantage of including a realistically evolving density distribution in our model.

We calculate the filling fraction of outflows using a Poisson distribution of sources and compare with our method of biasing AGN toward the high density regions within a cosmological simulation (see §2). We first calculate the porosity of AGN outflows at each redshift, given by:

$$Q(z) = \frac{4\pi}{3} \int_z^\infty \frac{dz'}{\tau_{AGN}} \frac{dt'}{dz'} \int_{L_{min}}^{L_{max}} R^3 \phi(L_B, z) f_{out} dL_B, \quad (6)$$

where the above quantities are calculated in physical units. We then calculate the filling fraction assuming a Poisson distribution:

$$f(z) = 1 - e^{-Q(z)}. \quad (7)$$

In the above calculations, we have determined the volume of each outflow under pressure equilibrium conditions, and under the assumption that the energy injection is instantaneous. The pressure is determined by the average particle density at each redshift and a constant

temperature of  $T = 1.5 \times 10^4$  K. We compare the above filling fraction with that produced by our model, as described in the previous section, for a simulated volume of  $128^3 h^{-3} \text{Mpc}^3$  (with  $0.5 h^{-1} \text{Mpc}$  cell resolution) in Figure 4. The Figure shows that the Poisson distribution of sources produces a higher filling fraction than our model. The simulation provides a realistic environment for each AGN. The outflows of AGN residing in regions of higher density do not fill as large a volume because the IGM exerts more pressure on the bubbles than in a uniform, average density distribution. Also, the AGN themselves are not distributed over as large a volume of space, as they tend toward higher density regions. Therefore, their outflows do not fill as large a fraction of the simulation as if they were uniformly distributed.

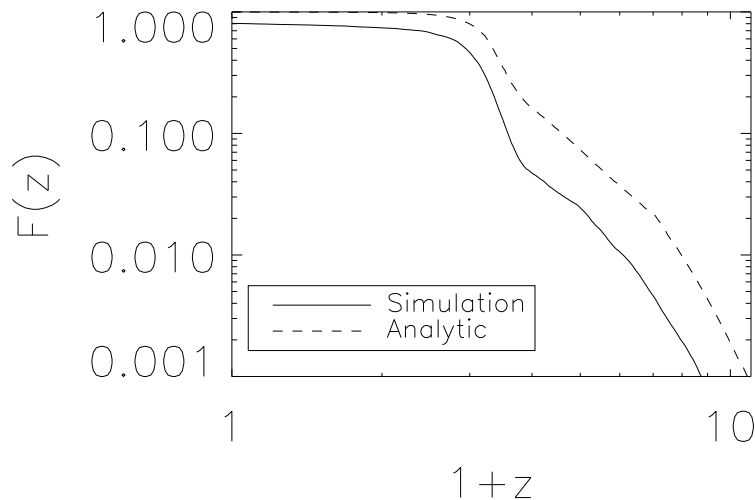


Fig. 4.— Filling fractions for a uniform density distribution (no density bias) and for an evolving density distribution (with density bias). The simple Poisson distribution results in a higher filling fraction than in the scenario accounting for an evolving density distribution.

## 5. RESULTS

We have seen in the previous two sections the general result of our model on the filling fraction of AGN outflows. In this section, we will examine the effects of varying simulation box size and resolution, AGN lifetime, and the distribution of AGN as determined by AGN bias. We will first conduct convergence studies, to determine the effects of box size and resolution on the rest of our analysis.

### 5.1. Convergence Studies

We ran our analysis on simulations of differing box sizes in order to choose the optimal box size for the rest of our studies. Larger boxes are more inclusive, but also much more computationally expensive, and so convergence is desirable. For each box size, we determine the fractional volume heated by AGN as a function of redshift using the model for bubble growth described in §3. We have evolved boxes of length  $64 h^{-1}$  Mpc,  $128 h^{-1}$  Mpc, and  $256 h^{-1}$  Mpc (each with  $1 h^{-1}$  Mpc cells) on a side. Figure 5 shows the filling fraction for each box size. The filling fraction does not vary dramatically between the two larger box sizes (for this reason, we did not complete the run for the largest, most expensive box size). It appears that we have reached convergence for the  $128 h^{-1}$  Mpc box. We therefore choose the  $128 h^{-1}$  Mpc box size for all of our parameter studies.

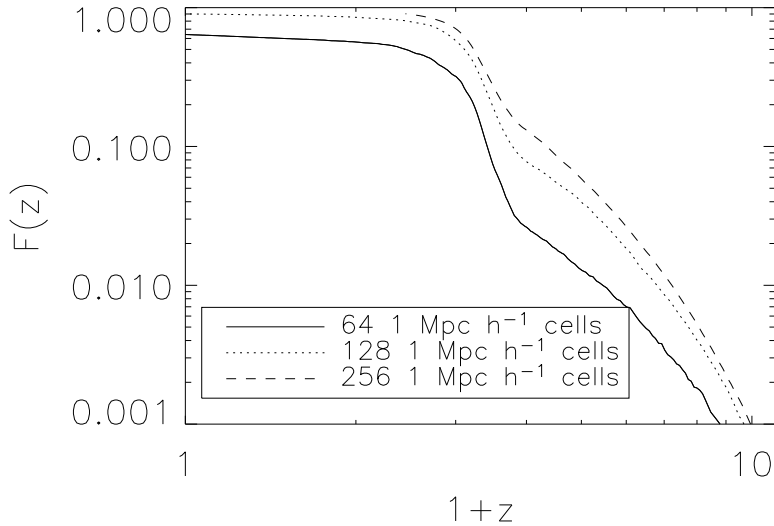


Fig. 5.— Filling fractions for different box volumes. Note that due to the computation time required for the  $256 h^{-1}$  Mpc length box, we did not calculate the filling fraction all the way to  $z = 0$ .

In addition to box size studies, we also examined the effects of simulation resolution on the AGN heated fractional volume. In simulations with finer resolution, individual cells can reach significantly higher densities (see Fig. 6), which directly affects the sizes of the bubbles in our simulations. The result is a different fractional volume affected by AGN depending on resolution. High resolution represents a more accurate picture of the simulated volume, but like large box size, is more computationally expensive because of the larger number of

cells. Therefore, we increase the resolution in our simulation box until the filling fraction no longer depends on resolution, after which, there is no need for finer resolution. We studied the  $64 h^{-1}$  Mpc length box with resolutions of  $1 h^{-1}$  Mpc cells,  $0.5 h^{-1}$  Mpc cells, and finally  $0.25 h^{-1}$  Mpc cells. We reach convergence in the filling fraction very quickly, as shown in Figure 7. The results for the  $0.5 h^{-1}$  Mpc cells and the  $0.25 h^{-1}$  Mpc cells are very similar, and so we choose the faster computation,  $0.5 h^{-1}$  Mpc cells, for our fiducial resolution.

## 5.2. AGN Lifetime

We have chosen for our fiducial model a constant lifetime for all AGN,  $\tau_{AGN} = 10^8$  yrs. Yu & Tremaine (2002) examine the dependence of lifetime on black hole mass and their results show modest variation in lifetime ( $\sim 30 - 300$  Myr) over the range of black hole masses of interest here. They determine AGN lifetime from a combination of the luminosity function and black hole number density, and their results are comparable to the associated Salpeter times, further evidence that black holes accrete most of their mass during their active phases. Our choice of  $\tau_{AGN} = 10^8$  yrs is consistent with their results. We test the effect of using higher and lower lifetimes as well. We apply a constant lifetime of  $10^7$  yrs as our lower limit. According to S & B,  $10^7$  yrs is an approximate lower limit for AGN lifetime, obtained from arguments similar to those of Yu & Tremaine:

$$f_{on}(z) = \frac{\tau_{AGN}}{t_{Hubble}} \geq \frac{\Phi(> L_B, z)}{n(> M_{BH}, z = 0)} . \quad (8)$$

In the above equation (eq. 22 of S & B), the AGN lifetime is determined from the fraction of galaxies having active nuclei at a given redshift ( $f_{on}$ ). This fraction can be determined by the ratio of the comoving number density of AGN (where  $\Phi$  is the number density of AGN with luminosities greater than  $L_B$  at redshift  $z$ ) to the black hole number density ( $n$ ). S & B assume that the black hole number density only increases with time, so that eq. 8, with the number density evaluated at  $z = 0$ , will give a minimum lifetime. For our upper limit, we use  $\tau_{AGN} = 10^9$  yrs, consistent with Croom et al. (2004) who determine an upper limit on AGN lifetime from arguments about the growth of dark matter halo mass. We do not examine redshift or mass dependence of  $\tau_{AGN}$ , because the variation is not significant over the range of lifetimes we consider.

We find that shorter lifetimes result in a lower filling fraction. In order to remain consistent with the luminosity function in the case of shorter lifetimes, many more AGN will become active at later redshifts than in the longer lifetime case. As AGN are born later in the simulation, they sit in regions of higher density than AGN born earlier, as the density

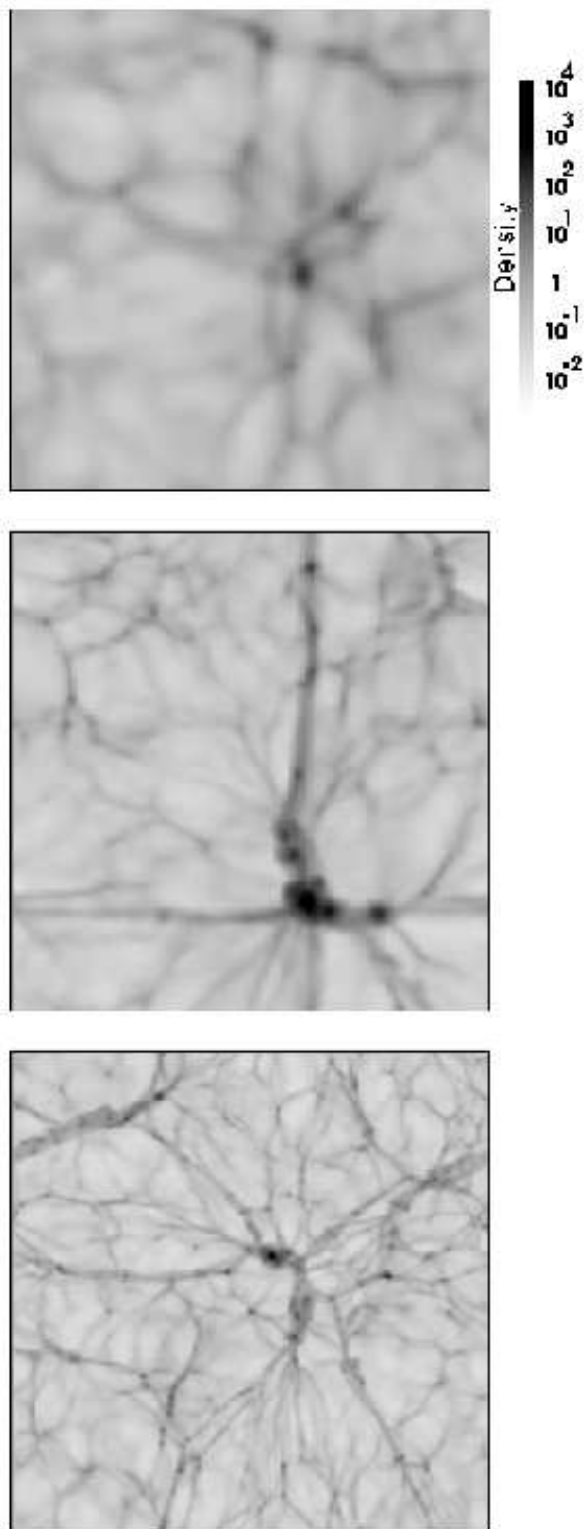


Fig. 6.— Examples of different resolutions. The above Figures show density distributions at  $z=0$  for different runs with differing resolutions. The upper box has  $1 \ h^{-1}$  Mpc cells, the center box has  $0.5 \ h^{-1}$  Mpc cells, and the lower box has  $0.25 \ h^{-1}$  Mpc cells. All boxes are  $64 \ h^{-1}$  Mpc across. A wider range of densities is reached for finer resolved boxes.



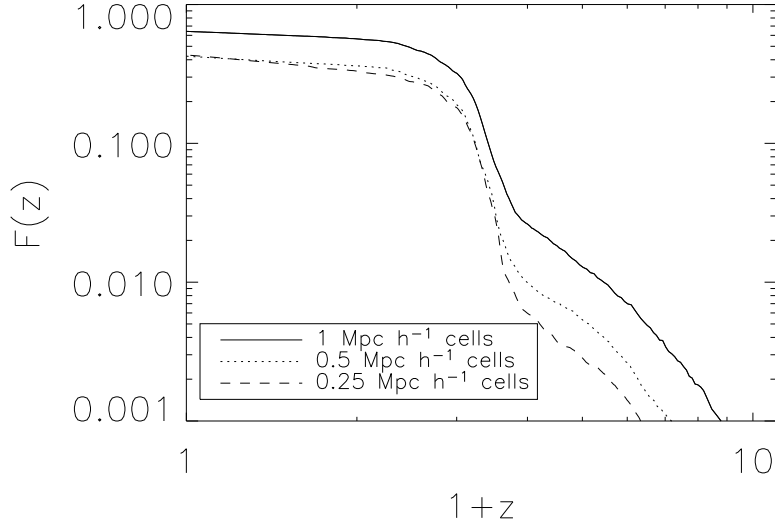


Fig. 7.— Filling fraction for different cell resolutions of a box of length  $64 h^{-1}$  Mpc. The two most finely resolved runs produce very similar results by  $z = 2$ , and so we choose  $0.5 h^{-1}$  Mpc cells as our fiducial resolution, as it is the more computationally inexpensive of the two.

distribution evolves with redshift. In this analysis, we have not included the possibility of recurrent activity associated with the same nucleus because the duty cycles of AGN are so low that it would introduce a small effect. Figure 8 shows  $F(z)$  for lifetimes of  $10^7$ ,  $10^8$ , and  $10^9$  yrs. In order to test that our interpretation of the effect of evolving density distribution is correct, we calculate  $F(z)$  for the three values of AGN lifetime under the assumption that the density distribution is uniform throughout the universe. Figure 9 shows the same range of lifetimes for the uniform density case. As expected, here we do not see the trend with lifetime because the density dependence has been removed. Therefore, because of the evolving density distribution, a shorter AGN lifetime will result in a lower filling fraction at  $z = 0$ .

### 5.3. AGN Bias

Observations show that AGN are biased toward regions of high density, with this bias increasing toward higher redshifts. A simple, quantitative implementation of this observed bias is the relation  $n_{AGN} \propto \rho_m^\alpha$ , where  $n_{AGN}$  is the number density of AGN in units of average number density of AGN, and  $\alpha$  is the linear bias parameter. Therefore,  $\alpha$  is a

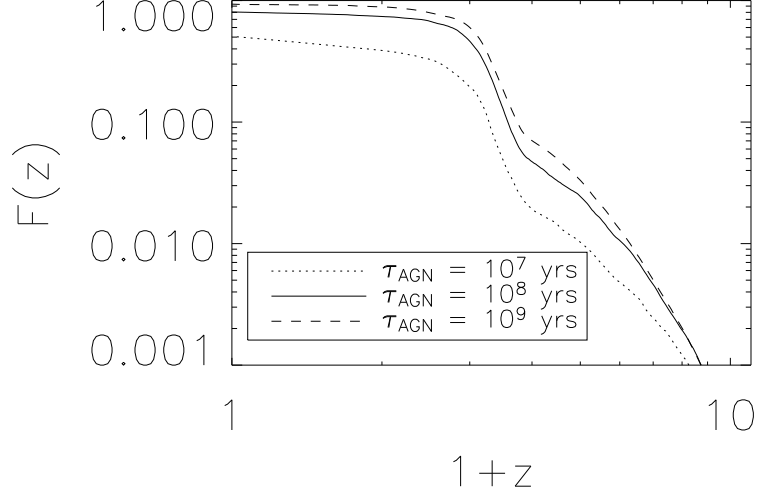


Fig. 8.— Filling fraction for different values of constant AGN lifetimes. Shorter AGN lifetimes imply younger AGN living in higher density environments.

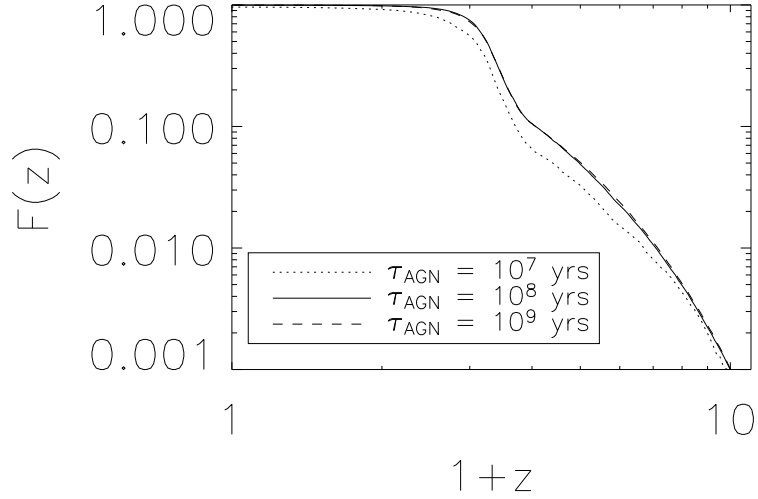


Fig. 9.— Filling fraction for different values of constant AGN lifetimes for a constant, isotropic density distribution. Without an evolving density distribution, lifetime does not strongly effect the filling fraction.

measure of the correlation between matter density and AGN density. We examine simple constant bias models here as well as one redshift dependent model. We do not, however, examine the possibility of luminosity dependent bias here, nor do we distinguish between the bias of radio-loud and radio-quiet QSOs despite evidence that radio-loud sources are more strongly clustered. Therefore, our bias parameter,  $\alpha$ , should be considered as an average bias of the outflow-producing population of AGN.

Our fiducial model was run with a constant bias,  $\alpha = 2$ , consistent with the average of many bias models. Because bias increases with redshift, we also ran a model with an increased constant bias of  $\alpha = 3$ . With a larger bias, AGN will be more tightly clustered to higher density regions, preventing their outflows from growing as large, and resulting in more overlap between bubbles. The result is a lower filling fraction, as shown in Figure 10.

Since the value of the bias parameter is not constant, but more likely to be (at the very least) redshift dependent, we have also tested the following redshift dependent model from Croom et al. (2004):

$$\alpha(z) = 0.53 + 0.289(1 + z)^2 . \quad (9)$$

The above is a simple model derived from 2dF data (up to  $z < 2.48$ ) combined with WMAP and 2dF cosmology. Rather than extrapolate this model over our entire redshift range, for  $z \geq 3$  we use a constant bias of  $\alpha = 5.154$ , determined by evaluating the above equation at  $z = 3$ . The effects of redshift dependent bias are seen in Figure 10. At higher redshifts, AGN are more strongly biased toward high density regions than in either of our constant bias models, and so the filling fraction is significantly lower. At lower redshifts ( $z \lesssim 1$ ), AGN are even less biased toward regions of high density than in our fiducial model, and so  $F(z)$  increases approaching  $z = 0$ .

## 6. DISCUSSION AND CONCLUSIONS

We have examined the filling fraction of AGN outflows in the context of large-scale cosmological simulations, and considered the influence of various observationally constrained parameters on the result. We find that the kinetic fraction of outflows need not be very high ( $\sim 10\%$ ) for AGN outflows to fill the entire IGM by  $z \sim 2$ . Observations of gaps in the Ly $\alpha$  forest provide possible constraints on the filling fraction, that can in turn be used to place constraints on the kinetic luminosity. In our study we have used a luminosity function consistent with optical surveys to distribute outflows throughout our simulation, however, future studies will have to consider X-ray surveys, which predict more faint luminosity AGN.

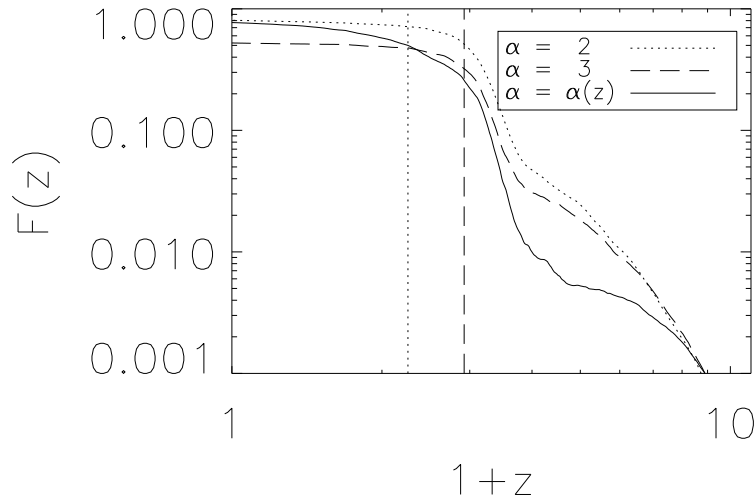


Fig. 10.— Comparison of filling fractions computed with different bias parameters. The two constant bias parameters are shown as well as a  $z$ -dependent bias described in §5.3. The two vertical lines correspond to the redshifts at which the functional form of the bias equals each of the constant biases (*dashed*:  $\alpha = 3$  and *dotted*:  $\alpha = 2$ )

Our model employs several simple approximations, but is nonetheless instructive. We have made the assumption that AGN outflows are spherical bubbles, propagating into the AGN adiabatically for a short while, until reaching pressure equilibrium with their environments. Spherical symmetry is not likely to remain intact once the outflow reaches far enough into the IGM. The outflows will expand away from large-scale structures, such as filaments, and into less dense regions. However, we can assume spherical symmetry as an average geometry, and the effects on the volume filling fraction are not likely to be very large. Our assumption that radiative cooling can be ignored is justified by the timescales involved. If we were to consider more complex environments in our model, such as those of clusters, we would need to include a great deal more physics (including cooling) requiring hydrodynamical simulations. While the actual outflow physics and geometry are likely to be more complex than we assume, our assumptions provide a good first-order approximation of the filling fraction of AGN.

The parameters we have studied, AGN lifetime, and AGN bias, contribute significantly to the AGN filling fraction as expected. We have assumed a particular evolution of the gas density distribution, in which the gas density profile is relatively uniform at high- $z$ , and forms high density filaments at low- $z$ . We have tested upper and lower limits for AGN

lifetime, and find that shorter AGN lifetimes result in a lower filling fraction than longer lived AGN due to the evolving gas density distribution. We have examined the effects of different AGN biases on filling fraction as well. Larger bias results in an ultimately lower filling fraction. However, bias likely depends on factors such as redshift and luminosity, and the dependence of the evolution of the filling factor on bias is likely to be more complicated than in our simple scenario. Changes both in the bias, and in the AGN lifetime affect the filling fraction of outflows because of the importance of the underlying density distribution and its importance for determining AGN distribution and environments.

We are very grateful to Mitch Begelman for his contributions to this paper. Additionally, we thank Nahum Arav, Jack Gabel, Mateusz Ruszkowski, Mike Shull, and John Stocke for helpful discussions. This work was supported by NSF grant AST-0134373 and by the National Computational Science Alliance under grant AST-020018N, and utilized the SGI Origin 2000 array and IBM P690 array at the National Center for Supercomputing Applications.

## REFERENCES

- Barger, A. J., Cowie, L. L., Mushotzky, R. F., Yang, Y., Wang, W.-H., Steffen, A. T., & Capak, P. 2005, *AJ*, 129, 578
- Begelman, M. C., Blandford, R. D., & Rees, M. J. 1984, *Rev. Mod. Phys.*, 56, 255
- Benson, A. J., & Madau, P. 2003, *MNRAS*, 344, 835
- Boyle, B. J., Shanks, T., Croom, S. M., Smith, R. J., Miller, L., Loaring, N., & Heymans, C. 2000, *MNRAS*, 317, 1014
- Brotherton, M. S., van Breugel, W., Smith, R. J., Boyle, B. J., Shanks, T., Croom, S. M., Miller, L., & Becker, R. H. 1998, *ApJ*, 505, L7
- Brüggen, M., & Kaiser, C. R. 2002, *Nature*, 418, 301
- Chiu, W. A., & Ostriker, J. P. 2000, *ApJ*, 534, 507
- Crenshaw, D. M., Kraemer, S. B., Boggess, A., Maran, S. P., Mushotzky, R., & Wu, C.-C. 1999, *ApJ*, 516, 750
- Cristiani, S., et al. 2005, in *ESO Astrophysics Symposia, Multiwavelength Mapping of Galaxy Evolution*, ed. A. Renzini & R. Bender (Berlin; New York: Springer)
- Croom, S. M., et al. 2004, *MNRAS*, 356, 415
- Davé, R., Hernquist, L., Katz, N., Weinberg, D. H. 1999, *ApJ*, 511, 521

- De Kool, M., Arav, N., Becker, R. H., Gregg, M. D., White, R. L., Laurent-Muehleisen, S. A., Price, T., & Korista, K. T. 2001, *ApJ*, 548, 609
- Duncan, R. C., Ostriker, J. P., & Bajtlik, S. 1989, *ApJ*, 345, 39
- Elvis, M., et al. 1994, *ApJS*, 95, 1
- Fan, X., et al. 2001a, *AJ*, 121, 54
- Fan, X., et al. 2001b, *AJ*, 122, 2833
- Furlanetto, S., & Loeb, A. 2001, *ApJ*, 556, 619
- Gallagher, S. C. 1999, *ApJ*, 519, 549
- Gallagher, S. C. 2001, *ApJ*, 546, 795
- Gnedin, N. Y. 2000, *ApJ*, 542, 535
- Hamann, F., Korista, K. T., & Morris S. L. 1993, *ApJ*, 415, 541
- Hewett, P. C., & Foltz, C. B. 2003, *AJ*, 125, 1784
- Hewett, P. C., Foltz, C. B., & Chaffee, F. H. 1995, *AJ*, 109, 1498
- Hewett, P. C., Foltz, C. B., & Chaffee, F. H. 2001, *AJ*, 122, 518
- Hui, L., & Haiman, Z. 2003, *ApJ*, 596, 9
- Kim, T.-S., Cristiani, S., & D’Odorico, S. 2002, *A&A*, 383, 747
- Krolik, J. H. 1999, *Active Galactic Nuclei* (Princeton: Princeton Univ. Press)
- McDonald, P., & Miralda-Escudé, J. 2001, *ApJ*, 549, L11
- McDonald, P., Miralda-Escudé, J., Rauch, M., Sargent, W. L. W., Barlow, T. A., & Cen, R. 2001, *ApJ*, 562, 52
- Menou, K., et al. 2001, *ApJ*, 561, 645
- Miller, M. C., & Ostriker, E. C. 2001, *ApJ*, 561, 496
- Mo, H. J., & Mao, S. 2004, *MNRAS*, 353, 829
- Morris, S. L. 1988, *ApJ*, 330, L83
- Nath, B., & Roychowdhury, S. 2002, *MNRAS*, 333, 145
- Navarro, J. F., Frenk, C. S., & White, S. D. 1997, *ApJ*, 490, 493
- Penton, S., Stocke, J. T., & Shull, J. M. 2004, *ApJS*, 152, 29
- Porciani, C., Magliocchetti, M., & Norberg, P. 2004, *MNRAS*, 355, 1010
- Ricotti, M., Gnedin, N. Y., & Shull, J. M. 2000, *ApJ*, 534, 41
- Ruszkowski, M., Brüggén, M., & Begelman, M. C. 2004, *ApJ*, 615, 675

- Scannapieco, E., & Oh, S. P. 2004, *ApJ*, 608, 62
- Schaye J., Theuns T., Rauch, M., Efstathiou G., & Sargent, W. L. W. 2000, *MNRAS*, 318, 817
- Schirber, M., & Bullock, J.S. 2003, *ApJ*, 584, 110
- Shapiro, P. R., Iliev, I. T., & Raga, A. C. 2004, *MNRAS*, 348, 753
- Somerville, R. S. 2002, *ApJ*, 572, 23
- Stocke, J. T., Morris, S. L., Weymann, R. J., & Foltz, C. B. 1992, *ApJ*, 396, 487
- Susa, H., & Umemura, M. 2004, *ApJ*, 600, 1
- Tassis, K., Abel, T., Bryan, G. L., & Norman, M. L. 2003, *ApJ*, 587, 13
- Tegmark, M., Silk, J., & Evrard, A. 1993, *ApJ*, 417, 54
- Theuns, T., Zaroubi, S., Kim, T., Tzanavaris, P., & Carswell, R. F. 2002, *MNRAS*, 332, 367
- Ulrich, M.-H. 1988, *MNRAS*, 230, 121
- Valageas, P., & Silk, J. 1999, *A&A*, 350, 725
- Weymann, R. J. 1997, in *ASP Conf. Ser. 128, Mass Ejection from AGN*, ed. N. Arav, I. Shlosman, & R. J. Weymann (San Francisco: ASP), 3
- Weymann, R. J., Morris, S. L., Foltz, C. B., & Hewett, P. C. 1991, *ApJ*, 373, 23
- Willott, C. J., Rawlings, S., Blundell, K. M., & Lacy, M. 1999, *MNRAS*, 309, 1017.
- Wyithe, J. S. B., & Loeb, A. 2003, *ApJ*, 595, 614
- Yu, Q., & Tremaine, S. 2002, *MNRAS*, 335, 965